

ORIGINAL RESEARCH

Association between ARID2 and RAS-MAPK pathway in intellectual disability and short stature

Eungu Kang,¹ Minji Kang,² Younghee Ju,³ Sang-Joon Lee,² Yong-Seok Lee,⁴ Dong-Cheol Woo,⁵ Young Hoon Sung,^{5,6} In-Jeoung Baek,^{5,6} Woo Hyun Shim,^{7,8} Woo-Chan Son,⁹ In Hee Choi,¹⁰ Eul-Ju Seo,^{10,11} Han-Wook Yoo,^{10,12} Yong-Mahn Han,³ Beom Hee Lee ^{10,12}

► Additional material is published online only. To view, please visit the journal online (<http://dx.doi.org/10.1136/jmedgenet-2020-107111>).

For numbered affiliations see end of article.

Correspondence to

Professor Beom Hee Lee, ¹, Seoul 138-736, Republic of Korea; bhlee@amc.seoul.kr
Professor Yong-Mahn Han; ymhan@kaist.ac.kr

Received 18 April 2020

Revised 3 August 2020

Accepted 26 August 2020

ABSTRACT

Background ARID2 belongs to the Switch/sucrose non-fermenting complex, in which the genetic defects have been found in patients with dysmorphism, short stature and intellectual disability (ID). As the phenotypes of patients with ARID2 mutations partially overlap with those of RASopathy, this study evaluated the biochemical association between ARID2 and RAS-MAPK pathway.

Methods The phenotypes of 22 patients with either an ARID2 heterozygous mutation or haploinsufficiency were reviewed. Comprehensive molecular analyses were performed using somatic and induced pluripotent stem cells (iPSCs) of a patient with ARID2 haploinsufficiency as well as using the mouse model of *Arid2* haploinsufficiency by CRISPR/Cas9 gene editing.

Results The phenotypic characteristics of ARID2 deficiency include RASopathy, Coffin-Lowry syndrome or Coffin-Siris syndrome or undefined syndromic ID. Transient ARID2 knockout HeLa cells using an shRNA increased ERK1 and ERK2 phosphorylation. Impaired neuronal differentiation with enhanced RAS-MAPK activity was observed in patient-iPSCs. In addition, *Arid2* haploinsufficient mice exhibited reduced body size and learning/memory deficit. ARID2 haploinsufficiency was associated with reduced IFITM1 expression, which interacts with caveolin-1 (CAV-1) and inhibits ERK activation.

Discussion ARID2 haploinsufficiency is associated with enhanced RAS-MAPK activity, leading to reduced IFITM1 and CAV-1 expression, thereby increasing ERK activity. This altered interaction might lead to abnormal neuronal development and a short stature.

INTRODUCTION

The Switch/sucrose non-fermenting (SWI/SNF) complex is a member of the family of ATP-dependent chromatin-remodelling complexes, which facilitates DNA transcription, replication and repair by increasing DNA accessibility.^{1,2} Based on the subunit composition, SWI/SNF can be divided into two subcomplexes: the BRG1-associated factor (BAF) and the polybromo-associated BAF (PBAF). AT-rich interaction domain (ARID)1A or ARID1B are core components of BAF, whereas ARID2 is a core subunit of PBAF. SMARCA2 (BRM) and SMARCA4 (BRG1) are mammalian homologues of yeast SWI and SNF that are the catalytic subunits of BAF and PBAF.^{3,4}

Germline heterozygous mutations in the genes of the SWI/SNF complex were implicated in neurodevelopmental disorders, including intellectual disability (ID) and autism spectrum disorder. The Nicolaides-Baraitser syndrome (NBS) is caused by mutations in SMARCA2,^{5,6} while the Coffin-Siris syndrome (CSS, OMIM135900) and CSS-like phenotypes result from mutations in ARID1A, ARID1B, SMARCA4, SMARCB1 and SMARCE1.^{7,8} Since the pathogenic variants of SWI/SNF-associated genes manifest in classic CSS, NBS and several other overlapping phenotypic spectra, ranging from syndromic ID to severe atypical CSS, the term ‘SWI/SNF-related intellectual disability disorders (SSRIDD)’ was suggested.^{9,10}

Recently, loss-of-function heterozygous mutations in ARID2 were reported in patients with ID, short stature and dysmorphic features.^{11–14} Notably, the ARID2-containing PBAF chromatin-remodelling complex responds to ligands, such as interferons, which are bound to its nuclear receptor.^{15,16} IFITM1 expression (MIM, 604456) is dependent on ARID2 expression and has an inverse association with ERK activation.¹⁷ IFITM1 interacts with caveolin-1 (CAV-1) on cell membranes, and this interaction subsequently inhibits ERK activation.¹⁸

Of note, a functional alteration, or gain-of-function in ERK is the molecular hallmark underlying Noonan syndrome (NS; OMIM 163950) and its related disorders, also referred to as RASopathy.¹⁹ RASopathy is one of the most common genetic disorder, characterised by dysmorphism, congenital heart defects, postnatal short stature and variable degrees of ID.^{20–22} RASopathy results from germline, gain-of-function and heterozygous mutations of the genes encoding the components of the RAS-MAPK signalling pathway.

In the current study, we evaluated the phenotypes of patients with either an ARID2 heterozygous mutation or with haploinsufficiency to identify the overlapping phenotypes between RASopathy and SSRIDD. Using the comprehensive molecular analyses of somatic and stem cells of a patient with ARID2 haploinsufficiency as well as the molecular and behavioural analyses of a mouse model of *Arid2* haploinsufficiency, the biochemical association between ARID2 and RAS-MAPK pathway and its relationship with ID was assessed.



© Author(s) (or their employer(s)) 2020. No commercial re-use. See rights and permissions. Published by BMJ.

To cite: Kang E, Kang M, Ju Y, et al. *J Med Genet* Epub ahead of print: [please include Day Month Year]. doi:10.1136/jmedgenet-2020-107111

PATIENTS AND METHODS

Patients

The clinical and genetic findings were reviewed for patients with either *ARID2* haploinsufficiency or loss-of-function mutation based on literature search.

In vitro transfection with shRNA

Skin fibroblasts (1.5×10^5 cells in 6-well plates) from a normal subject were transfected using the G-Fection transfection reagent (Genolution, Seoul, Korea) with 10 nmol of each shRNA-*ARID2* (MIM: 609539) (5'-CAGGAAUAGUGGAAUAGAUAGUGAUCUCACUAUCUAUUUCCACUAUCCUGUU-3'), shRNA-*ANO6* (MIM: 608663) (5'-GAAUACAUAACAAGAUAUUAUUGUCUCCAAUAUACUUCUUGUAUGUUAUUCUU-3'), shRNA-*TWF1* (MIM: 610932) (5'-GCUA GAAUUGUAGAAAGACAACUAUCUCUAGUUGUCUU CUACAAUUCUAGCUU-3') or non-specific control shRNA, according to the manufacturer's instructions.

Induced pluripotent stem cells establishment

Induced pluripotent stem cells (iPSCs) were established using the fibroblasts from patient 1 and from a normal control from a previous report,²³ as previously described.²⁴ The genomic deletion was evaluated using a human whole-genome $4 \times 180K$ CGH microarray.

ERK activation assay

The cells were starved for 24 hours prior to epidermal growth factor (EGF) (10 ng/mL) or basic fibroblast growth factor (FGF), (20 ng/mL) stimulation, as previously described.^{20,25} The levels of downstream signalling proteins were determined by western blot analysis. Primary antibodies included anti-ERK2 (1:1000, Cell Signaling Technology, Beverly, Massachusetts, USA), anti-Phospho-ERK antibodies (1:1000, Cell Signaling Technology), anti-RSP6 (1:1000, Genetex, Irvine, California, USA), anti-Phospho-RPS6 (1:1000, Genetex), anti-Akt (1:1000, Cell Signaling Technology) and anti-Phospho-Akt (1:1000, Cell Signaling Technology) antibodies. The relative ERK phosphorylation ratios were quantified using the LabWorks 4.6 software (UVP Products, Upland, California, USA) and normalised to total RAS, MEK1 and ERK expression. The experimental analyses were performed at least in triplicate.

Western blot analysis and immunofluorescence analysis

Total protein extracts (20 μ g) were resolved using SDS-PAGE (7.5%–10% vol/vol bisacrylamide-acrylamide mixed at a 37.5:1 ratio) and transferred on to nitrocellulose membranes and immunoblotted using specific antibodies. Primary antibodies included anti-*ARID2* (1:300, Genetex), anti-*CAV-1* (1:1000, Genetex), anti-*IFITM1* (1:1000, Genetex), anti- β -actin (1:2000, Bioworld, Dublin, Ohio, USA) and anti-*GAPDH* (1:2000, Enzo Life Sciences, Farmingdale, New York, USA) antibodies. Goat polyclonal rabbit IgG (Genetex) or mouse IgG (Genetex) was used as a secondary antibody. All experiments were performed thrice, and the means from triplicates were presented.

Human iPSCs established from patient 1 were fixed with 4% formalin at room temperature for 30 min, followed by permeabilisation in phosphate-buffered saline (PBS) containing 0.1% Triton X-100, and blocking with 3% bovine serum albumin (Sigma-Aldrich, St. Louis, Missouri, USA) for 1 hour at room temperature. The samples were incubated overnight with the following primary antibodies at 4°C: antibodies for *OCT4* (1:200, Santa Cruz Biotechnology, Dallas, Texas, USA), *SOX2* (1:200, Cell

Signaling Technology), *NANOG* (1:200, Cell Signaling Technology), *TRA-1-60* (1:200, Millipore), *TRA-1-80* (Millipore), *NESTIN* (1:100, Millipore), *SOX1* (1:300, R&D Systems, Minneapolis, Minnesota, USA), *NCAD* (1:200, BD Biosciences, San Jose, California, USA), *MAP2* (1:1000, Sigma-Aldrich) and *GFAP* (1:1000, Abcam, Cambridge, Massachusetts, USA). Cells were washed multiple times with PBS-T (0.1% Tween-20 in PBS) and incubated with Alexa Fluor 488-conjugated or Cy3-conjugated secondary antibodies (Invitrogen). Nuclei were observed by staining cells with DAPI (D9542, Sigma-Aldrich) for 10 min. Fluorescence was analysed using fluorescence microscopy (Olympus, Tokyo, Japan).

RAS-GTP activity assay

Active RAS (RAS-GTP) was detected through Raf1-RBD immunoprecipitation using the RAS activation kit (Millipore, Billerica, Massachusetts, USA) according to the manufacturer's instructions.

Generation of *Arid2* knockout mice using CRISPR/Cas9

To list the possible single guide RNAs (sgRNAs) specifically targeting mouse *Arid2* gene, the genomic DNA sequence (NC_000081 REGION: 96287522.96405463) was analysed using the web tool Benchling (<https://benchling.com/>). An sgRNA (5'-AGGCGCCTCCGGACGAGCGG-3') downstream of the translation start site of the *Arid2* gene showed a minimum of four off-target sequences (data not shown), and hence, was selected as a potentially specific sgRNA, based on a previous report.²⁶ Oligomers for the generation of an sgRNA template (5'-TAGGAGGCGCCTCCGGACGAGCGG-3' and 5'-AAACCCGCTCGTCCGGAGGCGCCT-3') were annealed and cloned into the *BsaI* sites of the pUC57-sgRNA vector (Addgene 51132). For the in vitro transcription, the template DNA was PCR-amplified using a pair of primers specific for the pUC57-sgRNA vector (M13F, 5'-GTAAAACGACGGCCAGT-3; pCAG-RGEN-R, 5'-GCACCGACTCGGTGCCACT-3), and the sgRNA was synthesised using the MEGAShortscript T7 kit (Ambion) according to the manufacturer's instructions. Cas9 mRNA was prepared by in vitro transcription from linearised pRGEN-Cas9-CMV plasmid (ToolGen, Seoul, Republic of Korea) using the mMACHINE T7 Ultra kit (Ambion) according to the manufacturer's instructions. C57BL/6N and ICR mice (Orient Bio, Republic of Korea) were used as embryo donors and foster mothers, respectively, and CRISPR/Cas9-mediated gene targeting in mice was performed as described previously (online supplemental figure S2).²⁷

Measurement of the frontal cortex thickness and the hippocampal volume

Ten each of adult *Arid2*^{+/-} and wild-type (WT) (\pm) mice were selected to identify dysmorphology. To assess the morphological changes *Arid2*^{+/-} mice, high-resolution coronal T2-weighted brain MRI was performed on the mice at the ages of 7–8 months in each of 10 WT and *Arid2*^{+/-} mice. The frontal cortex thickness, total brain thickness and both hippocampi volume in 1.94 mm anterior from the bregma were measured using ImageJ software, V1.51 (Bethesda, Maryland, USA, <https://imagej.nih.gov/ij/>).

Morris water maze test

The Morris water maze (MWM) consisted of a circular pool (130 cm in diameter, 35 cm high) that was filled with water and was made opaque by adding skim milk powder. A platform

(10 cm in diameter) was submerged 1.5 cm below the surface of the water, and a visual cue was placed near the platform. A video recorder positioned in the ceiling was connected to a tracking device (S-MART, Panlab, Barcelona, Spain). The animals were released into the pool at different points during four trials. The platform was then removed from the pool, and each animal was released into the pool for 1 min. The latency to first entry to reach the hidden platform, the number of platform crossings and total distance travelled were determined and analysed.

Open field test

The mice were placed in a square open field apparatus (35 cm×35 cm with 20 cm high walls), and their spontaneous locomotive activity was recorded for 10 min using a ceiling-mounted video camera. Each animal was tested only once, and the area was cleaned with 70% alcohol between tests. The total distance travelled (cm) and the time spent outside the central area (20 cm×20 cm) were analysed using a tracking device (S-MART, Panlab).

Statistics

All statistical analyses were performed using SPSS V.21 for Windows. Two-tailed independent t-tests were used to compare the data between the two groups; $p < 0.05$ was considered to be statistically significant.

RESULTS

Clinical and genetic characteristics of patients with ARID2 haploinsufficiency

The clinical and genetic findings were reviewed for 22 patients with either *ARID2* haploinsufficiency or intragenic mutation based on literature search (table 1 and online supplemental material, table S1).^{11–14 28–33}

Table 1 Summary of clinical features of 22 reported patients with 12q12 deletion or *ARID2* haploinsufficiency

Clinical features	12q12-13.11 deletions	Intragenic <i>ARID2</i> mutations	P value
Intrauterine growth restriction	4/8 (50%)	4/13 (30.8%)	0.646
Short stature	6/8 (75.0%)	11/14 (78.6%)	1.000
Developmental delay or intellectual disability	8/8 (100%)	14/14 (100%)	–
Microcephaly	4/8 (50.0%)	1/14 (7.1%)	0.039
Facial dysmorphism			
Coarse face	0/8 (0.0%)	5/14 (35.7%)	0.115
Frontal bossing	0/8 (0.0%)	6/14 (42.9%)	0.510
Down-slanting palpebral fissure	4/8 (50.0%)	6/14 (42.9%)	1.000
Ptosis	2/8 (25.0%)	2/14 (14.3%)	0.602
Broad nose	3/8 (37.5%)	3/14 (21.4%)	0.624
Low set and posteriorly rotated ear	8/8 (100%)	8/14 (57.1%)	0.051
High arched palate or cleft palate	6/8 (75.0%)	4/14 (28.6%)	0.074
Micrognathia or retrognathia	4/8 (50.0%)	8/14 (57.1%)	1.000
Congenital heart disease	3/8 (37.5%)	1/14 (7.1%)	0.117
Skeletal abnormalities	7/8 (87.5%)	10/14 (71.4%)	0.613
Fifth finger clinodactyly and/or nail hypoplasia	5/8 (62.5%)	7/13 (53.8%)	1.000
Clinical diagnosis			
Noonan syndrome or related disorders	6/8 (75.0%)	2/14 (14.3%)	0.008

Our patient (patient 1) belonged to the Korean RASopathy cohort (figure 1A and online supplemental figure S1). The patient was symptomatic for ID, short stature and had dysmorphic features with congenital anomalies. Dysmorphic craniofacial features were as followed: microcephaly, sparse hair and eyebrows, strabismus, myopia, hypertelorism, epicanthal folds, prominent upper lips, high-arched palate, low-set ears and a low posterior hairline. Simian creases on both hands and ichthyosis were also observed. Although RASopathy was suspected, *PTPN11*, *SOS1*, *KRAS*, *HRAS*, *NRAS*, *RAF1*, *BRAF*, *SHOC2*, *MAPK21*, *MAP2K2* and *SPRED1* genes were normal. Whole-exome sequencing was performed to exclude the possibility of another genetic disorder causing developmental delay (DD); however, a pathogenic, clinically relevant variant was not detected, whereas the chromosome microarray revealed that the patient 1 had a 3.7 Mb deletion at 12q12-13.11, chr12:43005992-46669000 (hg19).

Five other patients (patients 2–4, 7, 21) were reported to have deletions at chromosome 12q12-13.11, where *ARID2* is located.^{14 28–30 32} In addition, two siblings (patients 5 and 6) clinically diagnosed with NS had a balanced rearrangement of chromosome 12; ins(12)(q12p11.2p12.3)³¹ (online supplemental table S1 and figure 1A). In these siblings, one chromosomal break point was predicted to split the *ARID2* gene at intron 3.

In addition, 14 patients (patients 8–20, 22) were reported to harbour intragenic *ARID2* mutations, including eight frameshift mutations, four nonsense mutations and two large exonic deletions^{11–14 33} (online supplemental table S1 and figure 1B).

All 22 patients exhibited DD or ID along with a dysmorphic face (table 1). Other commonly shared features were skeletal abnormalities, including fifth finger clinodactyly (17/22, 77.3%) and short stature (17/22, 77.3 %). Their clinical diagnoses were heterogeneous, including RASopathy (8 patients), Coffin-Low syndrome or CSS (1 patient) or undefined syndromic DD or ID (13 patients). Regarding phenotypic differences between patients with 12q12-13.11 deletion and intragenic *ARID2* mutations, microcephaly, low set and posteriorly rotated ear and clinical diagnosis of NS or related disorders were more frequent in the patients with 12q12-13.11 deletions.

ARID2 haploinsufficiency is associated with enhanced RAS-MAPK pathway activity

To evaluate the downstream transcriptional effects of *ARID2* haploinsufficiency, we performed transient *ARID2* KO using shRNA in HeLa cells. shRNA-*ANO6* and shRNA-*TWF1*, which are included in the deletion region, chromosome 12q12 of patient 1, were selected as well to compare the effect of *ARID2* knockout (figure 2A–C).

Since the RASopathy phenotypes were shared among patients with *ARID2* deficiency, enhanced activity of the RAS-MAPK pathway, the biochemical hallmark of RASopathy, was investigated. The phosphorylation of ERK2 (pERK2), which is one of the final effectors in the RAS-MAPK pathway, increased significantly after EGF stimulation (10 ng/mL for 10 min) in the HeLa cells treated with shRNA-*ARID2*, whereas the pERK2 activity did not increase in those with shRNA-*ANO6* or shRNA-*TWF1* (figure 2D–F). This enhancement was similar to the increase in the pERK2 activity in fibroblasts of a patient with NS with a *PTPN11* mutation, p.Asn308Asp (online supplemental material 1, figure S1). Conversely, the activities of AKT and RPS6, which are the effectors of the AKT pathway and the mammalian target of rapamycin (mTOR) pathway, respectively, did not

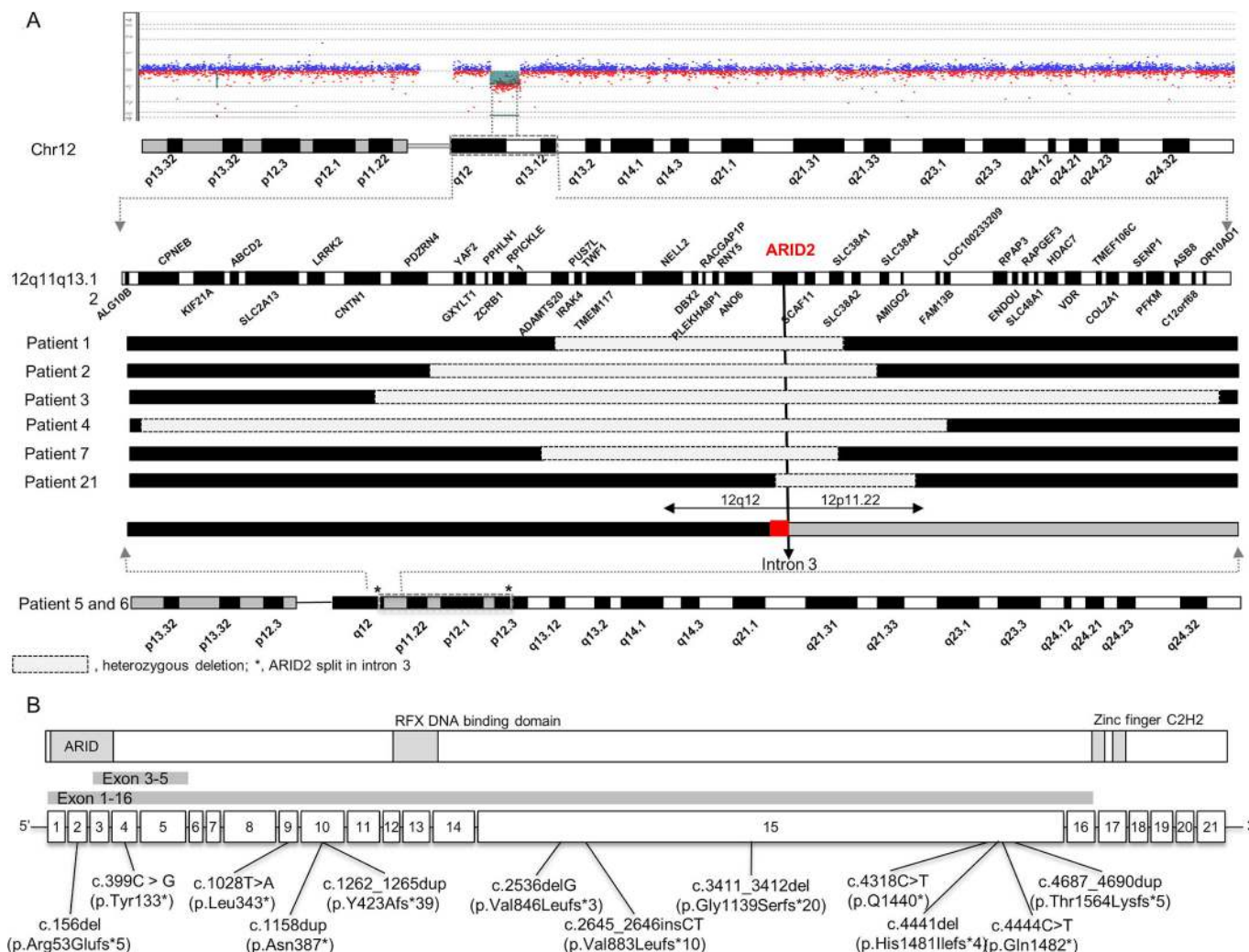


Figure 1 Genomic alterations in the patients with either an *ARID2* heterozygous mutation or haploinsufficiency. (A) Schematic representation of the 12q11 region and genes within this region. The genomic alterations are 12q12-13.11 deletion (Chr12:43005992-46669000, patient 1), 12q12 deletion (patient 2), 12q12-q13.12 deletion (patient 3), 12q11-q13 deletion (patient 4), 12q12 deletion (hg19 chr12:43,418,911-46,601,627, patient 7), 12q12-13.11 deletion (hg19 chr12:46189641-47575801, patient 21) and ins(12)(q12p11.2p12.3) (patients 5 and 6). In the two siblings, patients 4 and 5, with a balanced chromosomal rearrangement, ins(12)(q12p11.2p12.3), the break point on 12q12 was predicted to split *ARID2* at intron 3. (B) *ARID2* domain structure and the location of previously published *ARID2* mutations.

change after stimulation by EGF in the shRNA-*ARID2*-treated cells (figure 2G,H).

ARID2 haploinsufficiency is related to reduced expression of IFITM1 and CAV-1

IFITM1 (MIM, 604456) expression is dependent on *ARID2* expression and inversely associated with ERK activation.¹⁷ Additionally, IFITM1 interacts with CAV-1 on cell membranes, which subsequently inhibits ERK activation.¹⁸ CAV-1 is known to interact with PTPN11³⁴ and ERK.³⁵ Therefore, *ARID2* haploinsufficiency is expected to reduce IFITM1 expression, and the reduced interaction between IFITM1 with CAV-1 leads to enhanced ERK activity. To validate this hypothesis, we assessed the expression levels of IFITM1 and CAV-1 in fibroblasts from patient 1 and observed that the expression of IFITM1 and CAV-1 reduced significantly in the patient's fibroblasts compared with that in normal fibroblasts stimulated by EGF (10 ng/mL for 10 min) (figure 3A,B). Accordingly, the RAS-GTP/RAS ratio was significantly increased compared with that in normal fibroblasts (figure 3C).

Arid2 KO mice generated using CRISPR/Cas9: *Arid2*^{+/-} mice have reduced body size, thin frontal cortex and large hippocampus

The genomic DNA sequence of the mouse *Arid2* gene (NC_000081 REGION: 96287522.96405463) was selected for CRISPR/Cas9-mediated gene targeting in mice, as described previously.²⁷ Founder mice with frameshift mutations in the exon 1 of the *Arid2* gene were identified using the following primer pair: 5'-GCGTTTGAACCGCGATCT-3' and 5'-CAGG GATCTTCTTAAACGGCG-3'. The parental *Arid2*^{+/-} mice were backcrossed into C57BL/6 for over three generations. *Arid2*^{+/-} mice were tail genotyped (online supplemental material, figure S2). To exclude differences caused by sex, we used only male mice. Ten adult *Arid2*^{+/-} and 10 WT mice were selected to identify dysmorphology. A brain MRI scan was performed on mice aged 7–8 months.

Arid2 expression was reduced in the testes of *Arid2*^{+/-} mice, one of the major organs where *Arid2* is known to be expressed. We assessed the activity of the RAS-MAPK pathway by determining the levels of phosphorylated Shp2 (pShp2), Erk1 (pErk1)

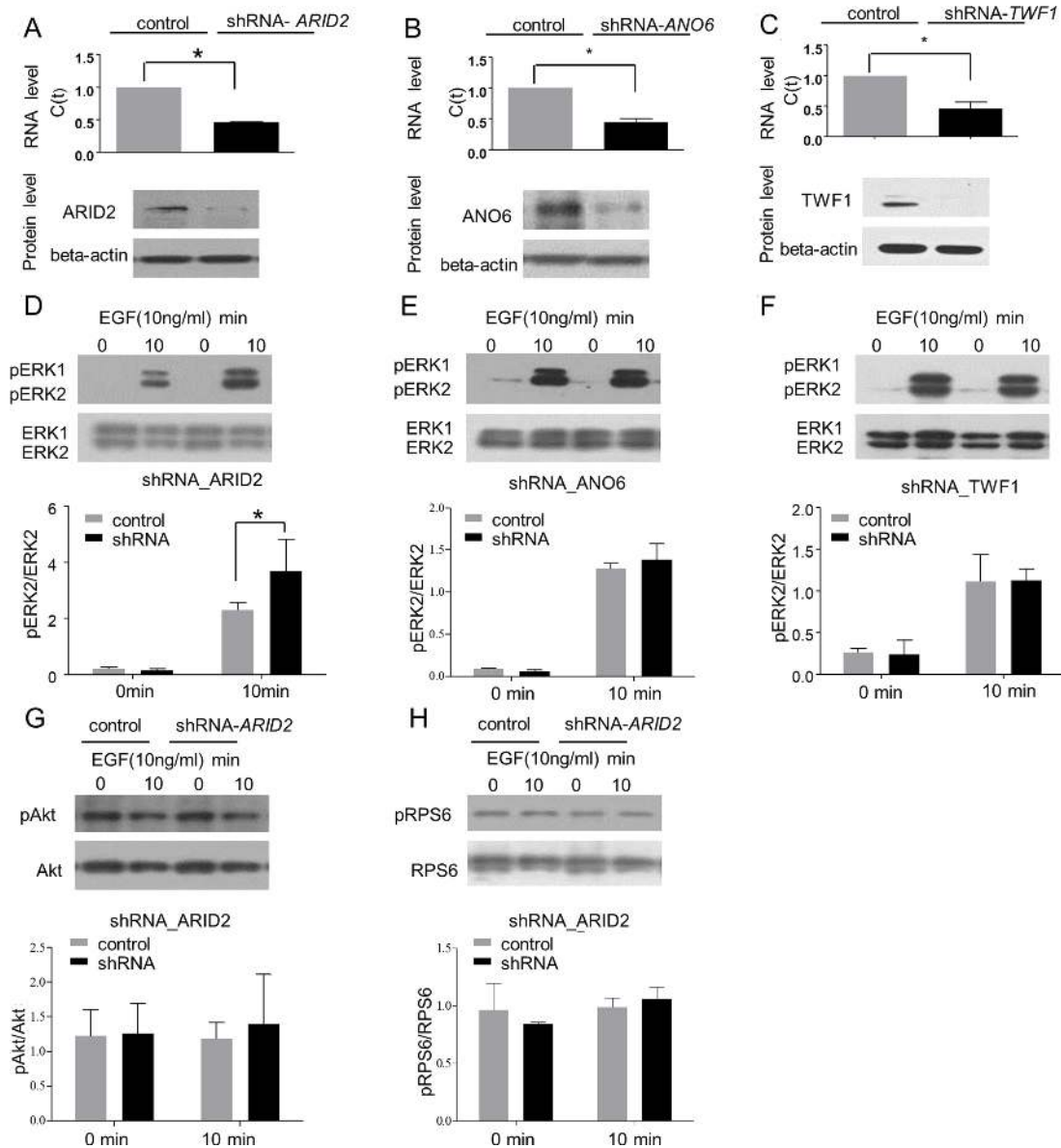


Figure 2 Transient knockout (KO) study using shRNA in HeLa cells. (A–C) The expression of ARID2, ANO6 and TWF1 after treatment with shRNA of each gene. (D–F) The ratio of phosphorylated ERK2 (pERK2) to total ERK2, the final effector of Ras-MAPK pathway activity, was significantly increased when treated with shRNA-ARID2 under epidermal growth factor (EGF) (10 ng/mL) stimulation. (G, H) No significant changes in the activity of AKT and mammalian target of rapamycin (mTOR) signalling pathway, which were represented by Akt and RSP6 levels, respectively, were observed after treatment with shRNA-ARID2. The p value was determined by two-tailed independent t-test. *P<0.05.

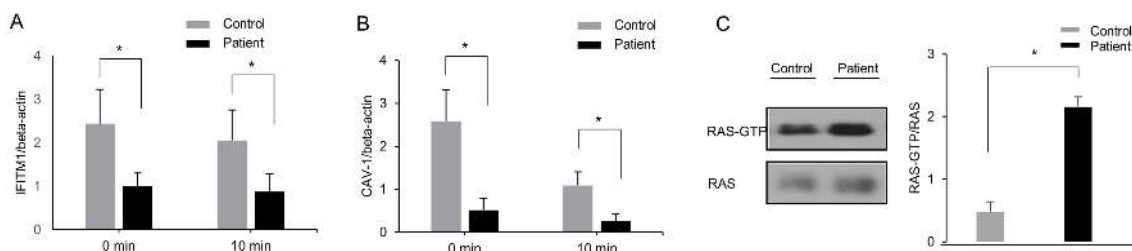


Figure 3 The expression of IFITM1 and caveolin-1 (CAV-1) in fibroblasts from patient 1 with ARID2 haploinsufficiency. (A, B) There was a reduction in the expression of IFITM1 and CAV-1, which is inversely related to ERK activation. (C) Ras-GTP activity increased significantly. The p value was determined by two-tailed independent t-test. *P<0.05.

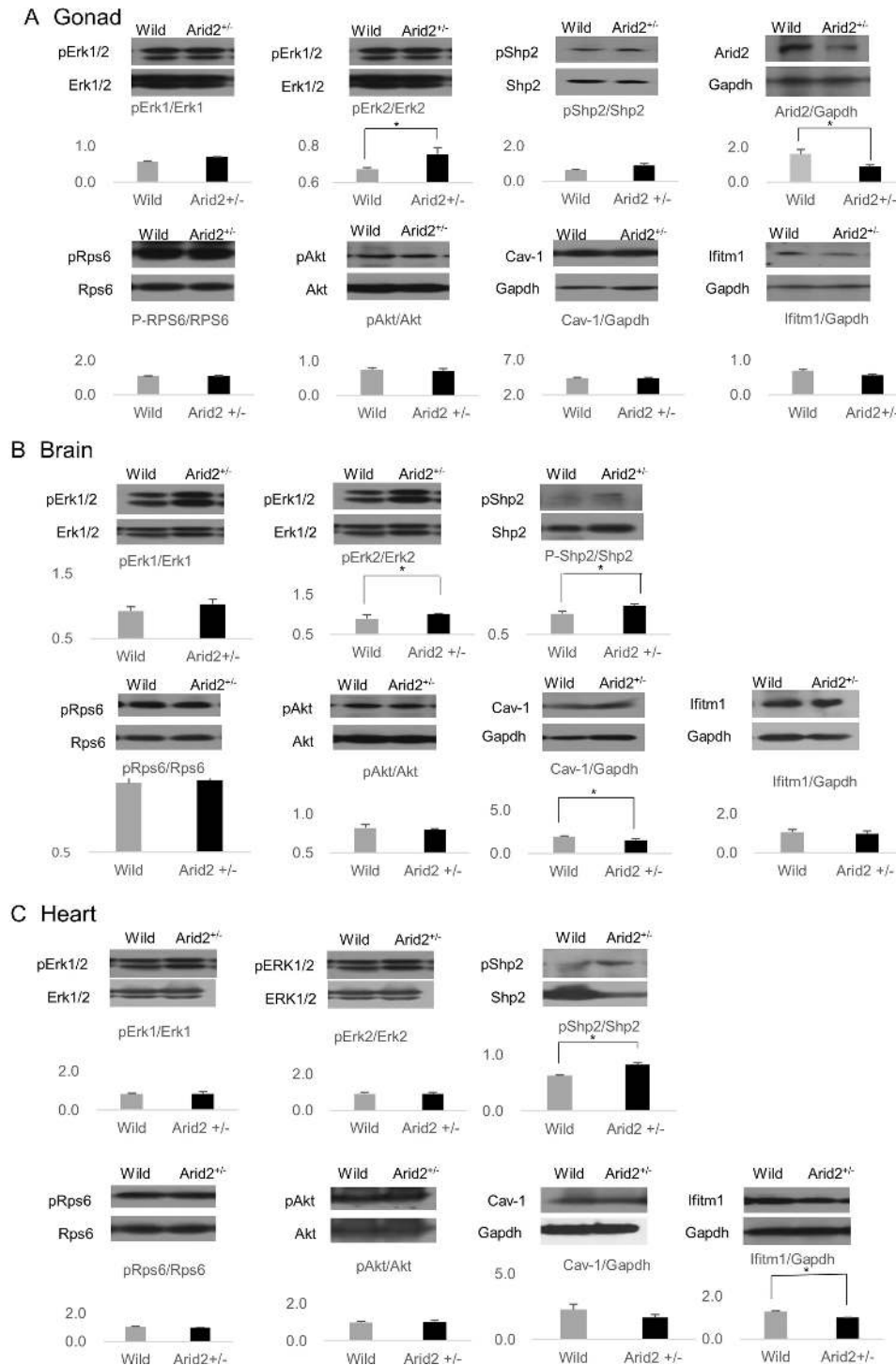


Figure 4 The expression of Arid2, caveolin-1 (Cav-1), Ifitm1 and the activity of Ras-MAPK pathway in gonad (A), brain (B) and heart (C) tissues of the *Arid2*^{+/-} and wild-type (WT) mice. (A) Phosphorylated Erk2 levels were significantly increased in gonad tissues from *Arid2*^{+/-} mice. (B) Phosphorylated Erk2 and Shp2 levels were significantly increased and the expression of Cav-1 was reduced in brain tissues from *Arid2*^{+/-} mice. (C) Phosphorylated Shp2 levels were increased and the expression of Ifitm1 was reduced in heart tissues from *Arid2*^{+/-} mice. The p value was determined by two-tailed independent t-test. *P<0.05.

and Erk2 (pErk2) in gonad (figure 4A), brain (figure 4B) and heart (figure 4C) tissues in *Arid2*^{+/-} WT mice. Compared with the levels in the WT mice, pShp2 levels were higher in the brain and heart tissues of *Arid2*^{+/-} mice, and pErk2 levels were higher in the gonad and brain tissues. Cav-1 and Ifitm1 levels were reduced in the brain and heart tissues, respectively (figure 4).

The *Arid2*^{+/-} mice could survive into adulthood and appeared healthy; however, there was a reduction in their weight (21.6±2.8 g vs 27.2±1.2 g, p<0.001) and nose-to-rump length (8.5±0.4 cm and 9.2±0.2, p<0.001) compared with that of the WT. The *Arid2*^{+/-} mice did not exhibit facial dysmorphism, gross organ defects and histological abnormalities in brain, heart

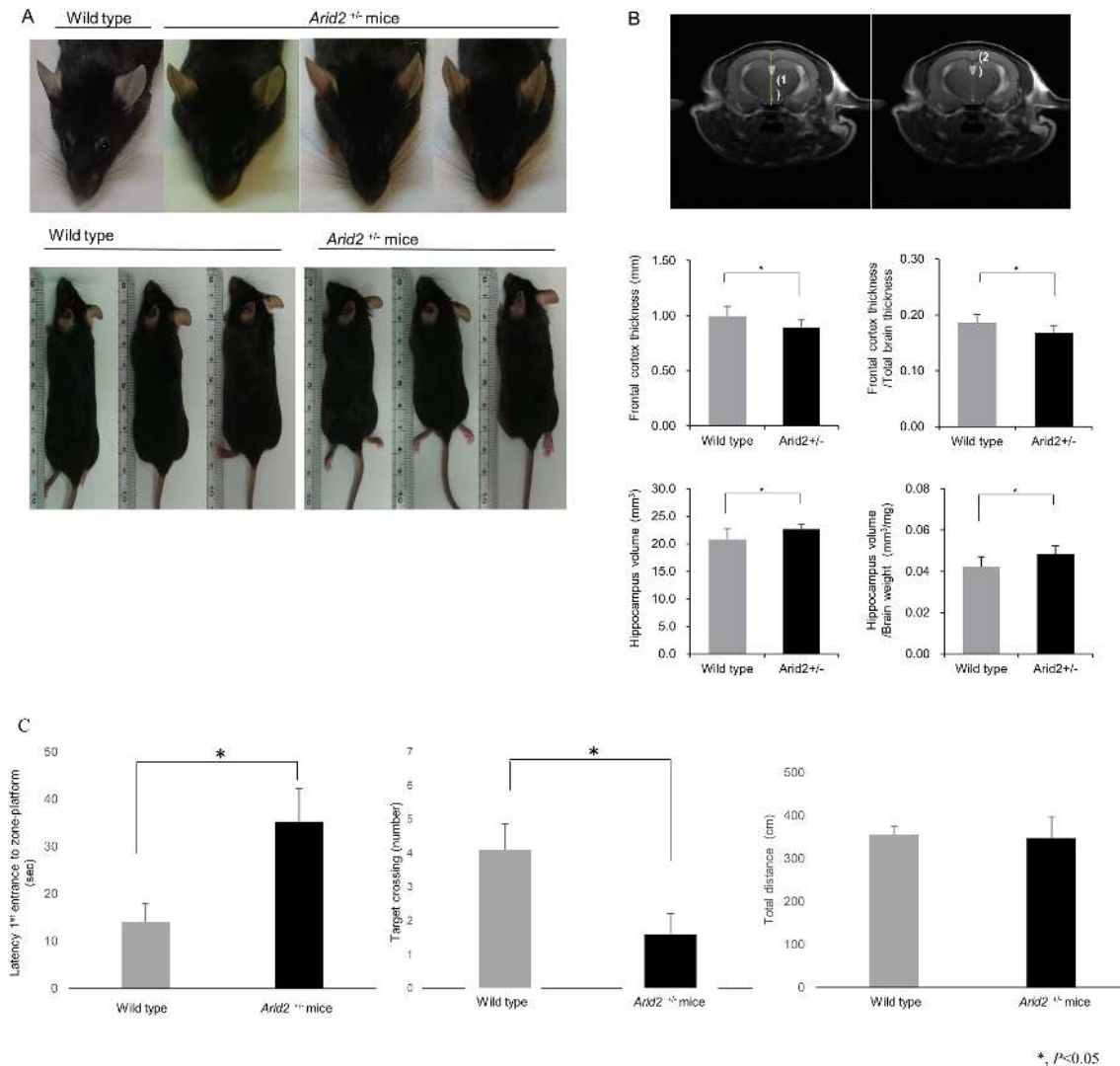


Figure 5 *Arid2*^{+/-} mice exhibited reduced body size and deficits in spatial learning and memory. (A) Facial morphology and body size of adult *Arid2*^{+/-} mice. (B) The axial T2-weighted images of the adult *Arid2*^{+/-} mice. The vertical lines indicated by (1) and (2) represent total brain thickness and thickness of frontal cortex, respectively. *Arid2*^{+/-} mice had thinner frontal cortex and larger hippocampus than wild-type (WT). (C) The results of Morris water maze test. The latency of first entry to reach the hidden platform was longer, and the number of platform crossings was reduced in the adult *Arid2*^{+/-} mice. The p value was determined by two-tailed independent t-test. **P*<0.05.

and testis, as revealed by the interorbital and pupillary distances measured using MRI (figure 5A). However, the frontal cortex thickness and the ratio of frontal cortex thickness-to-total brain thickness were significantly reduced in *Arid2*^{+/-} mice compared with those in the WT mice. The hippocampal volume and the ratio of the hippocampus volume to the total brain weight were higher in *Arid2*^{+/-} than in the WT mice (figure 5B).

Arid2^{+/-} mice exhibit deficits in spatial learning and memory

Hippocampal-dependent spatial learning and memory of the mice were assessed in MWM task. There were no differences in the total distances travelled in the MWM test between *Arid2*^{+/-} and WT mice (mean±SEM, 348.07±49.36 cm vs 356.51±19.45 cm, *p*=0.875). However, the latency to first entry to reach the hidden platform was longer in the adult *Arid2*^{+/-} mice (mean±SEM, 35.28±6.99 s vs 14.02±3.89 s, *p*=0.016), and the number of platform crossings reduced significantly in the adult *Arid2*^{+/-} mice (mean±SEM, 1.60±0.62 vs 4.10±0.77, *p*=0.021), indicating memory-related and learning-related defects in this group (figure 5C).

In the open field test, there were no differences in the total distances travelled and the time in zone-periphery (mean±SEM, 2483.80±218.34 cm vs 2157.81±93.66 cm, *p*=0.187 and 471.62±24.32 s vs 454.20±12.81 s, *p*=0.534, respectively) between the adult *Arid2*^{+/-} and WT mice, indicating that the *Arid2*^{+/-} mice did not exhibit anxiety-like behaviour.

Neural differentiation impairment in patient-iPSCs with ARID2 haploinsufficient individuals

To assess ARID2 haploinsufficiency and ERK2 activity in early neurodevelopmental stages, iPSCs were established using the fibroblasts from patient 1 (patient-iPSCs) and from two types of WT cells (WT1, hESCs and WT2, normal-iPSCs) from a previous study,²³ as previously described.²⁴ The patient-iPSCs exhibited typical ES-like round shape with clear boundary on mitomycin C-treated mouse embryonic fibroblasts (MEFs) (online supplemental material, figure S3A) and highly expressed alkaline phosphatase and representative pluripotent markers (OCT4, SOX2, NANOG, Tra-1-60 and Tra-1-81) (online supplemental

material, figure S3B,C). The cells had normal karyotypes (online supplemental material, figure S3D) and had potential to differentiate into three germ layer lineages including neural tissues, secretory glandular tissues and chondroid tissues (online supplemental material, figure S3E). The genomic deletion of 3.7 Mb at 12q12-13.11 (Chr12:43005992-46669000) was confirmed in the genomic DNA from iPSCs of patient 1 using a human whole-genome 4×180K CGH microarray (online supplemental material, figure S4). As in the fibroblasts, p-SHP2, activated HRAS and p-ERK-to-ERK ratio were increased in the iPSCs of patient 1 compared with those in the normal control when the patient-iPSCs were stimulated by basic FGF (20 ng/mL) (online supplemental figure S5). In addition, patient-iPSCs exhibited reduced CAV-1 and IFITM1 expression compared with normal control (online supplemental figure S5).

To assess the neurological developmental process, the patient-iPSCs were sequentially differentiated into embryoid bodies (EBs), neural rosettes (NRs), neural precursor cells (NPCs) and neural cells. The patient-iPSCs were differentiated to EBs for 4 days. Patient-EBs exhibited mixed morphologies, such as small round shapes or jagged appearances, compared with WT-EBs (figure 6A). They were differentiated into NRs for 8 days. Patient-NRs had immature neuroepithelial structures and showed low expression of neuroectodermal markers (NCAD, SOX1 and SOX2 except to NESTIN) compared with WT cells (figure 6B,C). When patient-iPSCs were incubated with bone morphogenetic protein and transforming growth factor beta inhibitors, the patient-iPSCs normally developed into EBs without morphological differences (figure 6D) and clearly differentiated into NRs, compared with WT-NRs (figure 6E). However, patient-EBs exhibited activated p-ERK activity and reduced CAV-1 and IFITM1 expression (figure 6F).

Patient-NRs followed usual developmental patterns and developed to neurosphere made with NPCs similar with WT cells (figure 6G). Representative neuroectodermal markers (NESTIN, SOX1 and SOX2) were expressed in patient-NPCs (figure 6H), whereas the p-ERK levels were higher in patient-NPCs compared with those in WT NPCs (figure 6I). The CAV-1 and IFITM1 expression was significantly decreased in patient-NPCs (figure 6I).

WT and patient-NPCs differentiated into neural cells for 21 days (figure 6J) and expressed a mature neuronal marker (MAP2) without a glial marker (GFAP) (figure 6K). The p-ERK activity was significantly higher in patient-neural cells compared with that in the WT-neural cells (figure 6L). Additionally, the patient-neural cells exhibited a significant reduction in CAV-1 and IFITM1 levels compared with WT-neural cells (figure 6L).

DISCUSSION

In this study, we demonstrated that the ARID2 genetic defect is associated with variable human neurodevelopmental disorders such as RASopathy, Coffin-Lowry syndrome, CSS or undefined syndromic DD or ID. Using comprehensive molecular analyses, we demonstrated that its haploinsufficiency is associated with enhanced RAS-MAPK activity; ARID2 KO by shRNA resulted in increased ERK activity that was associated with a reduction in IFITM1 and CAV-1 expression, thereby reducing ERK inhibition. This association was observed in an animal model for Arid2 haploinsufficiency as well, which exhibited reduced body size and a learning/memory deficit as well as increased Erk activity with a reduction in Ifitm1 and Cav-1 expression. Finally, the iPSCs from a patient with ARID2 haploinsufficiency exhibited abnormal neuronal differentiation. Notably, ARID2

haploinsufficiency was selectively associated with increased ERK activation. No significant changes were observed in other signalling pathways, such as the AKT and mTOR pathways.

The enhanced RAS-MAPK pathway is associated with ID, as the enhanced ERK signalling induces abnormal neuronal organisation and connectivity during development and affects long-term memory induction and the associated neuronal plasticity.³⁶ Therefore, it is plausible to hypothesise that ARID2 haploinsufficiency is associated with ID through enhanced ERK activation. This hypothesis is supported by documentation of the overlapping clinical phenotypes resulting from RASopathy and ARID2 haploinsufficiency. RASopathy is marked by several clinical features, including craniofacial dysmorphism (ie, hypertelorism, down-slanting palpebral fissures, ptosis and low-set ears), cardiac malformation, ocular, cutaneous and musculoskeletal abnormalities and increased cancer risk. Additionally, variable degrees of neurocognitive impairment, ranging from severe to null learning disabilities, are common as well.³⁷ Some individuals with ARID2 haploinsufficiency of intragenic mutations exhibit facial features that overlap with those of individuals with RASopathy (down-slanting palpebral fissures, frontal bossing, low-set posteriorly rotated ear and micrognathia/retrognathia DD and short stature).¹¹ Conversely, as ARID2 is a part of the SWI/SNF complex, patients with ARID2 mutations share phenotypical features with patients with CSS or SSRIDD, or CSS-like features, as in the patients with ARID1A, ARID1B, SMARCA4, SMARCB1 and SMARCE1 mutations^{7 8 12-14}: ID, short stature, coarse face, hypertrichosis, sparse scalp hair, a short fifth finger, nail hypoplasia and agenesis corpus callosum. The mouse model used in this study exhibited these phenotypes partially. Although facial dysmorphism was not apparent, ID and short stature were observable.

IFITM1 and CAV-1 are the possible intermediaries between ARID2 haploinsufficiency and increased ERK activity as demonstrated in patient's skin fibroblast and patient-iPSCs. However, the Ifitm1 expression was not reduced in the brain tissue of Arid2 haploinsufficient mice, although reduced expression of Cav-1 and increased Erk activity. In this regard, there might be other links between ARID2 haploinsufficiency and ERK activity and further studies are required.

The SWI/SNF complex plays a role in proper neurite outgrowth and maintenance by regulating coordinated alterations between the actin cytoskeleton and the microtubule network, which is critical in normal neural development and brain function.^{38 39} A previous study on Arid1b KO mice that exhibited anxiety-like behaviour, social behaviour deficits and learning/memory impairment, reported significantly reduced numbers and lengths of cortical GABAergic interneurons with normal density and distribution of pyramidal neurons, astrocytes and oligodendrocytes.⁴⁰ In addition, Arid1b haploinsufficiency led to multiple changes in genetic expression in the brain that were associated with neural development as well as psychological behaviour and developmental disorders.^{41 42} In our study, the Arid2 haploinsufficient mice displayed learning and memory deficits. The reduced volume of hippocampus has been known to related to learning/memory impairment, intellectual disabilities, however, some studies reported bilateral hippocampal hypertrophy in malformations of cortical development or neurodegenerative disease.^{43 44} Although we did not conduct a detailed histological examination, the significant reduction in the size of the cerebral cortex and a large hippocampal volume further support the role of ARID2 in brain development.

Short stature and ID are common phenotypical features of RASopathy, SSRIDD and ARID2 haploinsufficiency. In this

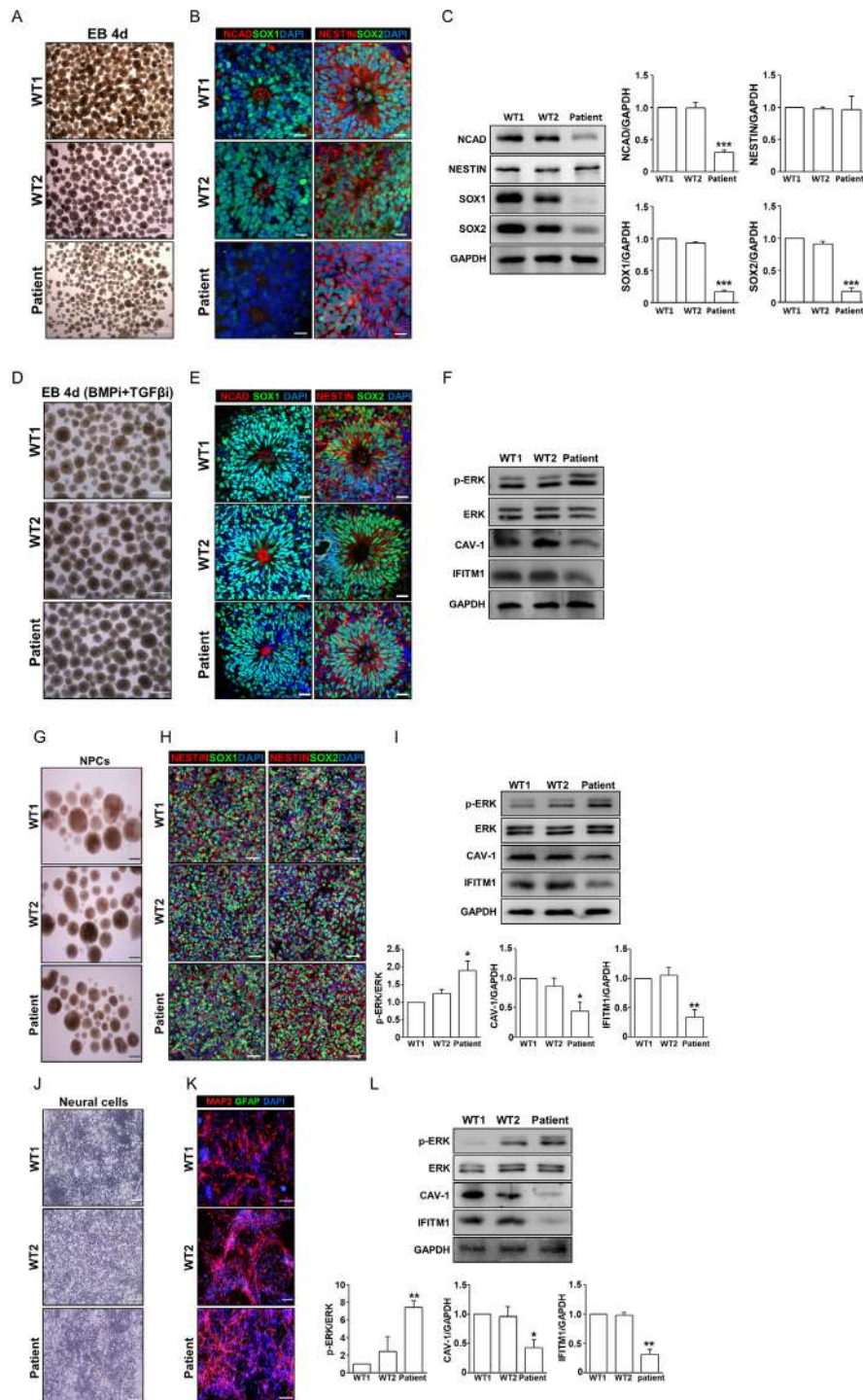


Figure 6 The neural differentiation of induced pluripotent stem cells (iPSCs) generated from patient 1 fibroblasts. (A) The embryoid bodies (patient-EBs) derived from patient-iPSCs exhibited aberrant morphologies on day 4 during EB maintenance. Scale bar, 500 μ m. (B and C) Neural rosettes (NRs) developed from patient-EBs revealed apparently immature neuro-epithelial structures and abnormal expression of neuroectodermal markers (NCAD, SOX1 and SOX2 except NESTIN). Scale bar, 20 μ m. Relative band intensities were expressed as mean \pm SEM (n=3). (D) Patient-EBs recovered morphologically when patient-iPSCs were incubated with bone morphogenetic protein (BMP) and transforming growth factor beta (TGF β) inhibitors (5 μ M dorsomorphin and 10 μ M SB431542) for 4 days during EB formation. Scale bar, 100 μ m. (E) Rescued patient-EBs normally differentiated into NRs that clearly expressed neuroectodermal markers (NCAD, SOX1, SOX2 and NESTIN). Scale bar, 20 μ m. (F) Patient-EBs exhibited elevated phosphorylated ERK activity and reduced caveolin-1 (CAV-1) and IFITM1 expressions. (G) Patient-NRs developed normally into neural precursor cells (NPCs) that were round. Scale bar, 200 μ m. (H) Dissociated patient-NPCs expressed neuroectodermal markers including SOX1, SOX2 and NESTIN. Scale bar, 50 μ m. (I) Patient-NPCs exhibited enhanced p-ERK activity and reduced CAV-1 and IFITM1 expressions. Relative band intensities are expressed as mean \pm SEM (n=3). (J) Patient-NPCs ordinarily differentiated into neural cells (patient-neural cells), as observed. Scale bar, 100 μ m. (K) Patient-neural cells expressed a mature neuronal marker (MAP2) similar to WT-neural cells and did not express a glial marker (GFAP). Scale bar, 100 μ m. (L) The Patient-neural cells also exhibited increased p-ERK activity and reduced CAV-1 and IFITM1 expressions. Relative band intensities were expressed as mean \pm SEM (n=3). The p value was determined by two-tailed independent t-test. *P<0.05, **p<0.01, ***p<0.001.

study, the mouse model with *Arid2* haploinsufficiency exhibited reduced body weight and length. The growth hormone-releasing hormone (GHRH)-growth hormone-insulin-like growth factor 1 (IGF-1) deficiency might be a major contributor of growth retardation; reduced plasma IGF-1 protein levels along with normal response to GHRH stimulation and no change in *Gnrh* mRNA level in the hypothalamus.^{41 45 46} Reduced IGF-1 level (105 ng/mL, -1.21 SD score) was noted in the patient 1 as well.

In conclusion, *ARID2* haploinsufficiency is associated with enhancement of the RAS-MAPK pathway, which subsequently contributes to the development of phenotypical features such as ID and short stature in affected patients. In addition, the study, for the first time, revealed the novel molecular connections among neurodevelopmental genetic disorders, SSRIDD and RASopathy, previously considered as distinct disease entities. This might provide new insights for future studies on the development of pharmacological interventions. Indeed, the reposition of the medications targeting the intracellular signalling pathway from oncological diseases into genetic dysmorphic disorders has been shown successful in certain diseases such as neurofibromatosis type 1 and PIK3CA-related overgrowth syndrome.^{47 48}

Author affiliations

- ¹Department of Pediatrics, Korea University Ansan Hospital, Ansan, Gyeonggi-do, Republic of Korea
- ²Asan institute for Life Sciences, Asan Medical Center, University of Ulsan College of Medicine, Seoul, Republic of Korea
- ³Department of Biological Sciences, Korea Advanced Institute of Science and Technology (KAIST), Daejeon, Republic of Korea
- ⁴Department of Physiology, Biomedical Sciences, Neuroscience Research Institute, Seoul National University College of Medicine, Seoul, Republic of Korea
- ⁵Convergence Medicine Research Center, Asan Institute for Life Sciences, Asan Medical Center, University of Ulsan College of Medicine, Seoul, Republic of Korea
- ⁶Department of Convergence Medicine, Bio-Medical Institute of Technology, Asan Medical Center, University of Ulsan College of Medicine, Seoul, Republic of Korea
- ⁷Department of Medical Science, Asan Medical Institute of Convergence Science and Technology, Asan Medical Center, University of Ulsan College of Medicine, Seoul, Republic of Korea
- ⁸Department of Radiology, Asan Medical Center, University of Ulsan College of Medicine, Seoul, Republic of Korea
- ⁹Department of Pathology, Asan Medical Center, University of Ulsan College of Medicine, Seoul, Republic of Korea
- ¹⁰Medical Genetics Center, Asan Medical Center, Seoul, Republic of Korea
- ¹¹Department of Laboratory Medicine, Asan Medical Center, University of Ulsan College of Medicine, Seoul, Republic of Korea
- ¹²Department of Pediatrics, Asan Medical Center, University of Ulsan College of Medicine, Seoul, Republic of Korea

Acknowledgements The authors would like to thank the patient and her family for participating in this study. The authors would like to thank the Magnetic Resonance Core Facility at the Convergence Medicine Research Center (CREDIT) of Asan Medical Center for MRI acquisition and analysis, and the Biomedical Computing core facility at the CREDIT of Asan Medical Center for support and instrumentation.

Contributors BHL, Y-MH and H-WY designed this study. MK and YJ performed most of the experiments. EK, MK, Y-SL, W-CS and YJ analysed the data. S-JL, Y-SL, D-CW, YHS, I-JB, WHS and W-CS performed some of the experiments. EK, IHC, E-JS, H-WY and BHL were involved in the diagnosis and treatment of the patient. EK, MK, YJ and BHL drafted and all authors revised the manuscript. All authors read and approved the final manuscript.

Funding This research was supported in part by the Bio & Medical Technology Development Programme of the national research Foundation (NRF) funded by the Korean government (NRF-2016M3A9B4915706 and NRF-2018M3A9H1078335).

Competing interests None declared.

Patient consent for publication Not required.

Ethics approval This study was approved by the Institutional Review Board of the Asan Medical Center, Seoul, Korea (IRB number 2016-0768). The patient and her parents provided written informed consent to genetic testing.

Provenance and peer review Not commissioned; externally peer reviewed.

Data availability statement All data relevant to the study are included in the article or uploaded as supplementary information.

ORCID iD

Beom Hee Lee <http://orcid.org/0000-0001-9709-2631>

REFERENCES

- 1 Zofall M, Persinger J, Kassabov SR, Bartholomew B. Chromatin remodeling by ISW2 and SWI/SNF requires DNA translocation inside the nucleosome. *Nat Struct Mol Biol* 2006;13:339–46.
- 2 Kassabov SR, Zhang B, Persinger J, Bartholomew B. SWI/SNF unwraps, slides, and rewraps the nucleosome. *Mol Cell* 2003;11:391–403.
- 3 Schuettengruber B, Bourbon H-M, Di Croce L, Cavalli G. Genome regulation by polycomb and trithorax: 70 years and counting. *Cell* 2017;171:34–57.
- 4 Kadoch C, Crabtree GR. Mammalian SWI/SNF chromatin remodeling complexes and cancer: mechanistic insights gained from human genomics. *Sci Adv* 2015;1.
- 5 Van Houdt J, Nowakowska BA, Sousa SB, van Schaik BDC, Seuntjens E, Avonce N, Sifrim A, Abdul-Rahman OA, van den Boogaard M-JH, Bottani A, Castori M, Cormier-Daire V, Deardorff MA, Filges I, Fryer A, Fryns J-P, Gana S, Garavelli L, Gillissen-Kaesbach G, Hall BD, Horn D, Huylebroeck D, Klapecki J, Krajewska-Walasek M, Kuechler A, Lines MA, Maas S, Macdermot KD, McKee S, Magee A, de Man SA, Moreau Y, Morice-Picard F, Obersztyen E, Pilch J, Rosser E, Shannon N, Stolte-Dijkstra I, Van Dijk P, Vilain C, Vogels A, Wakeling E, Wiczorek D, Wilson L, Zuffardi O, van Kampen AHC, Devriendt K, Hennekam R, Vermeesch JR. Heterozygous missense mutations in SMARCA2 cause Nicolaides-Baraitser syndrome. *Nat Genet* 2012;44:445–9.
- 6 Nicolaides P, Baraitser M. An unusual syndrome with mental retardation and sparse hair. *Clin Dysmorphol* 1993;2:232–6.
- 7 Coffin GS, Siris E. Mental retardation with absent fifth fingernail and terminal phalanx. *Am J Dis Child* 1970;119:433–9.
- 8 Koshi T, Okamoto N, Coffin-Siris Syndrome International Collaborators. Genotype-Phenotype correlation of Coffin-Siris syndrome caused by mutations in SMARCB1, SMARCA4, SMARCE1, and ARID1A. *Am J Med Genet C Semin Med Genet* 2014;166C:262–75–75.
- 9 Bögershausen N, Wollnik B. Mutational landscapes and phenotypic spectrum of SWI/SNF-related intellectual disability disorders. *Front Mol Neurosci* 2018;11:252.
- 10 Koshi T, Okamoto N, Ohashi H, Tsurusaki Y, Imai Y, Hibi-Ko Y, Kawame H, Homma T, Tanabe S, Kato M, Hiraki Y, Yamagata T, Yano S, Sakazume S, Ishii T, Nagai T, Ohta T, Niikawa N, Mizuno S, Kaname T, Naritomi K, Narumi Y, Wakui K, Fukushima Y, Miyatake S, Mizuguchi T, Saito H, Miyake N, Matsumoto N. Clinical correlations of mutations affecting six components of the SWI/SNF complex: detailed description of 21 patients and a review of the literature. *Am J Med Genet A* 2013;161A:1221–37.
- 11 Shang L, Cho MT, Retterer K, Folk L, Humberson J, Rohena L, Sidhu A, Saliganan S, Iglesias A, Vitazka P, Juusola J, O'Donnell-Luria AH, Shen Y, Chung WK. Mutations in ARID2 are associated with intellectual disabilities. *Neurogenetics* 2015;16:307–14.
- 12 Bramswig NC, Caluseriu O, Lüdecke H-J, Bolduc FV, Noel NCL, Wieland T, Surowy HM, Christen H-J, Engels H, Strom TM, Wiczorek D. Heterozygosity for ARID2 loss-of-function mutations in individuals with a Coffin-Siris syndrome-like phenotype. *Hum Genet* 2017;136:297–305.
- 13 Van Paemel R, De Bruyne P, van der Straaten S, D'hondt M, Fränkel U, Dheedene A, Menten B, Callewaert B. Confirmation of an ARID2 defect in SWI/SNF-related intellectual disability. *Am J Med Genet A* 2017;173:3104–8.
- 14 Gazdag G, Blyth M, Scurr I, Turmpenny PD, Mehta SG, Armstrong R, McEntagart M, Newbury-Ecob R, Tobias ES, Joss S. Extending the clinical and genetic spectrum of ARID2 related intellectual disability. A case series of 7 patients. *Eur J Med Genet* 2019;62:27–34.
- 15 Agalioti T, Lomvardas S, Parekh B, Yie J, Maniatis T, Thanos D. Ordered recruitment of chromatin modifying and general transcription factors to the IFN-beta promoter. *Cell* 2000;103:667–78.
- 16 Liu H, Kang H, Liu R, Chen X, Zhao K. Maximal induction of a subset of interferon target genes requires the chromatin-remodeling activity of the BAF complex. *Mol Cell Biol* 2002;22:6471–9.
- 17 Yang G, Xu Y, Chen X, Hu G. IFITM1 plays an essential role in the antiproliferative action of interferon-gamma. *Oncogene* 2007;26:594–603.
- 18 Xu Y, Yang G, Hu G. Binding of IFITM1 enhances the inhibiting effect of caveolin-1 on ERK activation. *Acta Biochim Biophys Sin* 2009;41:488–94.
- 19 Aoki Y, Niihori T, Narumi Y, Kure S, Matsubara Y. The RAS/MAPK syndromes: novel roles of the RAS pathway in human genetic disorders. *Hum Mutat* 2008;29:992–1006.
- 20 Lee BH, Kim J-M, Jin HY, Kim G-H, Choi J-H, Yoo H-W. Spectrum of mutations in Noonan syndrome and their correlation with phenotypes. *J Pediatr* 2011;159:1029–35.
- 21 Nava C, Hanna N, Michot C, Pereira S, Pouvreau N, Niihori T, Aoki Y, Matsubara Y, Arveiler B, Lacombe D, Pasmant E, Parfait B, Baumann C, Héron D, Sigaudy S, Toutain A, Rio M, Galonberg A, Leheup B, Verloes A, Cavé H. Cardio-facio-cutaneous and Noonan syndromes due to mutations in the RAS/MAPK signalling pathway: genotype-phenotype relationships and overlap with Costello syndrome. *J Med Genet* 2007;44:763–71.

- 22 Noonan JA. Hypertelorism with Turner phenotype. A new syndrome with associated congenital heart disease. *Am J Dis Child* 1968;116:373–80.
- 23 Kim H, Kim D, Jang M-J, Han Y-M. Variations in the epigenetic regulation of lineage-specific genes among human pluripotent stem cell lines. *Biochem Biophys Res Commun* 2012;424:331–7.
- 24 Takahashi K, Tanabe K, Ohnuki M, Narita M, Ichisaka T, Tomoda K, Yamanaka S. Induction of pluripotent stem cells from adult human fibroblasts by defined factors. *Cell* 2007;131:861–72.
- 25 Carvajal-Vergara X, Sevilla A, D'Souza SL, Ang Y-S, Schaniel C, Lee D-F, Yang L, Kaplan AD, Adler ED, Rozov R, Ge Y, Cohen N, Edelmann LJ, Chang B, Waghray A, Su J, Pardo S, Lichtenbelt KD, Tartaglia M, Gelb BD, Lemischka IR. Patient-specific induced pluripotent stem-cell-derived models of LEOPARD syndrome. *Nature* 2010;465:808–12.
- 26 Cho SW, Kim S, Kim Y, Kweon J, Kim HS, Bae S, Kim J-S. Analysis of off-target effects of CRISPR/Cas-derived RNA-guided endonucleases and nickases. *Genome Res* 2014;24:132–41.
- 27 Sung YH, Kim JM, Kim H-T, Lee J, Jeon J, Jin Y, Choi J-H, Ban YH, Ha S-J, Kim C-H, Lee H-W, Kim J-S. Highly efficient gene knockout in mice and zebrafish with RNA-guided endonucleases. *Genome Res* 2014;24:125–31.
- 28 Failla P, Romano C, Reitano S, Di Benedetto D, Grillo L, Fichera M, Castiglia L. 12q12 deletion: a new patient contributing to genotype-phenotype correlation. *Am J Med Genet A* 2008;146A:1354–7.
- 29 Tonoki H, Saitoh S, Kobayashi K. Patient with del(12)(q12q13.12) manifesting abnormalities compatible with Noonan syndrome. *Am J Med Genet* 1998;75:416–8.
- 30 Gallego M. A new case of interstitial 12q deletion. *Int Pediatr* 2000;15:37–40.
- 31 Yatsenko SA, del Valle Torrado M, Fernandes PH, Wiszniewska J, Gallego M, Herrera J, Bacino CA. Molecular characterization of a balanced rearrangement of chromosome 12 in two siblings with Noonan syndrome. *Am J Med Genet A* 2009;149A:2723–30.
- 32 Weng Y, Luo X, Hou L. Deletion at 12q12 increases the risk of developmental delay and intellectual disability. *Ann Hum Genet* 2018;82:482–7.
- 33 Khazanchi R, Ronspies CA, Smith SC, Starr LJ. Patient with anomalous skin pigmentation expands the phenotype of ARID2 loss-of-function disorder, a SWI/SNF-related intellectual disability. *Am J Med Genet A* 2019;179:808–12.
- 34 Caselli A, Mazzinghi B, Camici G, Manao G, Ramponi G. Some protein tyrosine phosphatases target in part to lipid rafts and interact with caveolin-1. *Biochem Biophys Res Commun* 2002;296:692–7.
- 35 Hua H, Munk S, Whiteside CI. Endothelin-1 activates mesangial cell ERK1/2 via EGF-receptor transactivation and caveolin-1 interaction. *Am J Physiol Renal Physiol* 2003;284:F303–12.
- 36 San Martín A, Pagani MR. Understanding intellectual disability through RASopathies. *J Physiol Paris* 2014;108:232–9.
- 37 Rauen KA. The RASopathies. *Annu Rev Genomics Hum Genet* 2013;14:355–69.
- 38 Bachmann C, Nguyen H, Rosenbusch J, Pham L, Rabe T, Patwa M, Sokpor G, Seong RH, Ashery-Padan R, Mansouri A, Stoykova A, Staiger JF, Tuoc T. mSWI/SNF (BAF) complexes are indispensable for the neurogenesis and development of embryonic olfactory epithelium. *PLoS Genet* 2016;12:e1006274.
- 39 Weinberg P, Flames N, Sawa H, Garriga G, Hobert O. The SWI/SNF chromatin remodeling complex selectively affects multiple aspects of serotonergic neuron differentiation. *Genetics* 2013;194:189–98.
- 40 Jung E-M, Moffat JJ, Liu J, Dravid SM, Gurumurthy CB, Kim W-Y. Arid1b haploinsufficiency disrupts cortical interneuron development and mouse behavior. *Nat Neurosci* 2017;20:1694–707.
- 41 Celen C, Chuang J-C, Luo X, Nijem N, Walker AK, Chen F, Zhang S, Chung AS, Nguyen LH, Nassour I, Budhipramono A, Sun X, Bok LA, McEntagart M, Gevers EF, Birnbaum SG, Eisch AJ, Powell CM, Ge W-P, Santen GW, Chahrouh M, Zhu H. *Arid1b* haploinsufficient mice reveal neuropsychiatric phenotypes and reversible causes of growth impairment. *Elife* 2017;6. doi:10.7554/eLife.25730. [Epub ahead of print: 11 Jul 2017].
- 42 Shibutani M, Horii T, Shoji H, Morita S, Kimura M, Terawaki N, Miyakawa T, Hatada I. Arid1b haploinsufficiency causes abnormal brain gene expression and autism-related behaviors in mice. *Int J Mol Sci* 2017;18:1872.
- 43 Kim H, Mansi T, Bernasconi N. Disentangling hippocampal shape anomalies in epilepsy. *Front Neurol* 2013;4:131.
- 44 Li W, Li K, Guan P, Chen Y, Xiao Y, Lui S, Sweeney JA, Gong Q. Volume alteration of hippocampal subfields in first-episode antipsychotic-naïve schizophrenia patients before and after acute antipsychotic treatment. *Neuroimage* 2018;20:169–76.
- 45 Binder G. Noonan syndrome, the Ras-MAPK signalling pathway and short stature. *Horm Res* 2009;71(Suppl 2):64–70.
- 46 David A, Hwa V, Metherell LA, Netchine I, Camacho-Hübner C, Clark AJL, Rosenfeld RG, Savage MO. Evidence for a continuum of genetic, phenotypic, and biochemical abnormalities in children with growth hormone insensitivity. *Endocr Rev* 2011;32:472–97.
- 47 Dombi E, Baldwin A, Marcus LJ, Fisher MJ, Weiss B, Kim A, Whitcomb P, Martin S, Aschbacher-Smith LE, Rizvi TA, Wu J, Ershler R, Wolters P, Therrien J, Glod J, Belasco JB, Schorry E, Brofferio A, Starosta AJ, Gillespie A, Doyle AL, Ratner N, Widemann BC. Activity of selumetinib in neurofibromatosis type 1-related plexiform neurofibromas. *N Engl J Med* 2016;375:2550–60.
- 48 Venot Q, Blanc T, Rabia SH, Berteloot L, Ladraa S, Duong J-P, Blanc E, Johnson SC, Huguin G, Boccara O, Sarnacki S, Boddaert N, Pannier S, Martinez F, Magassa S, Yamaguchi J, Knebelmann B, Merville P, Grenier N, Joly D, Cormier-Daire V, Michot C, Bole-Feyssot C, Picard A, Soupre V, Lyonnet S, Sadoine J, Slimani L, Chaussain C, Laroche-Raynaud C, Guibaud L, Broissand C, Amiel J, Legendre C, Terzi F, Canaud G. Targeted therapy in patients with PIK3CA-related overgrowth syndrome. *Nature* 2018;558:540–6.